IEEE Access
Multidisciplinary | Rapid Review | Open Access Journal

Received June 28, 2018, accepted August 21, 2018, date of publication August 30, 2018, date of current version September 28, 2018.

Digital Object Identifier 10.1109/ACCESS.2018.2867940

Noise Suppression Using Amplitude-Shaping OCDM With 16-Chip Multi-Level Phase-Shifted En/Decoder

RACHATA MANEEKUT AND PASU KAEWPLUNG
Department of Electrical Engineering, Faculty of Engineering, Chulalongkorn University, Bangkok 10330, Thailand
Corresponding author: Pasu Kaewplung (pasu.k@chula.ac.th)

This work was supported by the 90th Anniversary of Chulalongkorn University through the Rachadapisek Sompote Fund.

ABSTRACT We propose an amplitude-shaping (AS) technique to shape an en/decoded signal in 10-Gb/s coherent time-spreading optical-code division multiplexing (OCDM) with ON–OFF keying modulation format, using 16-chip multi-level phase-shifted keying en/decoders. By employing this technique, the primary beat noise and the multiple access interference can be suppressed, and the code detection performance is improved. The bit error rate and the power penalty of the 8 × 10 Gb/s AS-OCDM, obtained from the calculation and the simulation, are improved, in comparison with the conventional OCDM system.

INDEX TERMS Amplitude shaping, fiber to the home, optical code division multiplexing, passive optical network, time-spreading.

I. INTRODUCTION

The increase in the demand of data communication is growing rapidly since the number of end-subscribers is also growing up, and many types of widespread internet services such as the online gaming, the telemedicine service, the HDTV, and the 4K (also 8K) super hi-vision digital video format have been developed. These services bring dramatically huge amount of bandwidth [1], [2]. Furthermore, the evolution in wireless communication with the emergence 5G technology which expects the data rate of more than 10 gigabits per second (Gbps), are keys to increase the traffic in a back-haul communication link as well [3], [4]. Nevertheless, the bottleneck in data rate becomes a limitation at the fiber access network, since the cost as well as the complexity of the fiber access network should be as low as possible [5]. Currently, one of the main solutions to satisfy such the bandwidth hunger and to support the access span of the 5G radio access network (RAN) efficiently, is the fiber to the home (FTTH) based passive optical network (PON) [6]–[8]. Recently, the general requirements of 40G-PON with the major architecture platform employing the prospective time-wavelength division multiplexing has been announced in the name of next generation PON stage 2 (NG-PON2) [9], [10]. Furthermore, IEEE has recently discussed to launch a standardization of a 100-Gbps based Ethernet PON (100G-EPON) [11], [12].

Optical code-division multiplexing (OCDM) is one of an attractive scheme that can enhance the system performance of the next generation PON [13]. The en/decoding process is performed in optical domain. Therefore, it does not need any high electrical chip-rate processing devices. This scheme allows subscribers to transmit their own data over the same spectrum simultaneously. Therefore, each subscriber can obtain the maximum data rate without any bandwidth sharing. Moreover, subscribers can access to the network without contention as a truly asynchronous manner [14]–[16].

In the past few years, the coherent time-spreading (TS) OCDM using the multiport en/decoder based array waveguide grating (AWG), and the superstructure fiber Bragg grating (SSFBG) which are fabricated with the multi-level phase-shifted keying code, or Fourier code, have been used in many coherent OCDM systems, due to the great power contrast ratio (PCR≈ -13 to -23 dB) [17]–[20]. Therefore, the correlation property is excellent so that it can suppress the crosstalk among subscribers effectively. Many OCDM works have been successfully demonstrated based on data rates of 1.25-40 Gbps/subscriber, and the total data rates are ranged from 80-300 Gbps [13], [18], [19]. The signal deterioration caused by the chromatic dispersion can be suppressed by the narrow-band optical band-pass filter (NB-OBPF). Therefore, the OCDM-PON with the dispersion compensation-free

under the long-reach access span was demonstrated in [20]. Moreover, in 2011, the OCDM signal transmission with the largest capacity of 2.56 Tbps over 50 km was successfully demonstrated [21].

Nevertheless, the primary beat noise (PBN) and the multiple access interference (MAI) are the crucial problems that limit the BER and degrade the receiver sensitivity [22], [23]. The development of the optical en/decoder and the signal processing is the main key to improve the OCDM system performance. The low-cost 8-chip 320-Gchip/s apodized SSFBG was proposed for a 40 Gbps system to reduce the variability of the envelope of the encoded signal. It has shown with superior performance than the uniform SSFBG [24]. Moreover, the sample profile SSFBG has been shown to increase the code detection performance among several types of the SSFBG [13]. The research group in [25] and [26] has proposed two solutions to suppress the MAI and the PBN for the 10-Gbps OCDM-PON. The first solution, they used the extremely narrow-band optical band pass filter (ENB-OBPF) which resulting in the improvement of the BER performance of the filtered signal. For second solution, they proposed the use of 2 additional cascaded AWGs at the remote node (RN), so that they were able to transmit all 16 codes generated by the AWG simultaneously. Nevertheless, the solutions in [25] and [26] may be not suitable for some scenarios because the implementation of both the ENB-OBPF and the additional cascaded AWGs may increase system cost and complexity.

In this paper, we propose an alternative solution to improve the code detection performance of the coherent TS-OCDM PON. We apply a technique called amplitude-shaping (AS) to adjust the amplitude of the optical signal at the en/decoder to form a Gaussian shape profile for the first time to our knowledge. With this modification, the correlation property can be enhanced without using other additional external optical devices. We present the system performance of our approach by the numerical calculation and validate our results by a simulation. The results show that the BER and the receiver sensitivity of the AS-OCDM, with the appropriate shaping profile, are improved in comparison with the conventional OCDM system.

The paper is organized as follows. In section II, we introduce the AS-OCDM. In section III, we show the code detection performance as a function of the shaping profile. In section IV, we evaluate the BER performance without dispersion effect of both the AS-OCDM with the optimal value, and the conventional OCDM, respectively. Finally, in section V, we validate our numerical results with the software simulation.

II. AMPLITUDE-SHAPING OCDM SYSTEM

We introduce the amplitude-shaping (AS), to improve the code detection performance of the coherent OCDM system using multi-level phase-shifted code. The profile of the encoded signal can be shaped in the simplified Gaussian form as,

$$g(k) = a \exp\left[-\frac{(k-b)^2}{2w^2}\right], \tag{1}$$

where a is the maximum peak of the encoded signal, b is the center of the encoded signal, and w is the bell-shape Gaussian root-mean-square (RMS) width of the encoded signal, respectively [27], [28]. In a case that the ratio of b/w is converged to zero, all amplitudes are equal to a. On the other hand, by increasing the ratio b/w, the amplitudes will be formed in the bell-shape. Finally, all amplitudes tend to be all zero as the ratio b/w is increased to infinity. Fig. 1 shows 16 amplitudes of the Gaussian shaping profile with w. Each amplitude is normalized with the highest peak in that case. We can see clearly that all amplitudes in the case $w = 1000$ have the same level of 1. For the case $w = 10$, both left and right sides are slightly attenuated and we can see that all amplitudes are attenuated, then formed a beautiful bell-shape in the case $w = 2$, respectively. Finally, the case $w = 0.1$ shows two peaks with amplitude 1 at the center whereas others are equal to 0.

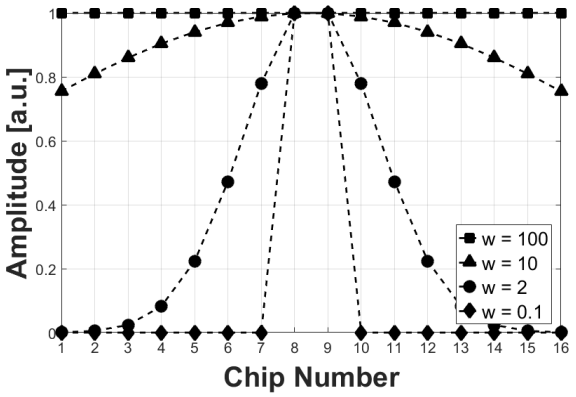

FIGURE 1. Normalized amplitudes of the encoded signal with different width.

The impulse response and the transfer function of the en/decoder using Fourier code which are corresponding to the Gaussian shaping profile are,

$$h_{code-c}(t) = \sum_{k=0}^{N-1} \sqrt{g(k+1)} \times \exp\left[-j\frac{2\pi k}{N}(c-1)\right] \cdot \delta(t - k\frac{T_{bit} \cdot SBR}{N}), \tag{2}$$

$$H_{code-c}(f) = \sum_{k=0}^{N-1} \sqrt{g(k+1)} \times \exp\left[-j2\pi k\left(\left(\frac{c-1}{N}\right) + f\frac{T_{bit} \cdot SBR}{N}\right)\right]. \tag{3}$$

Here, N is the total chip number. c is the code number. The term SBR is the ratio between total encoding period and the bit period, which is defined as $SBR = N \cdot t_{chip}/T_{bit}$, where T_{bit} is the bit period and t_{chip} is the chip period, respectively.

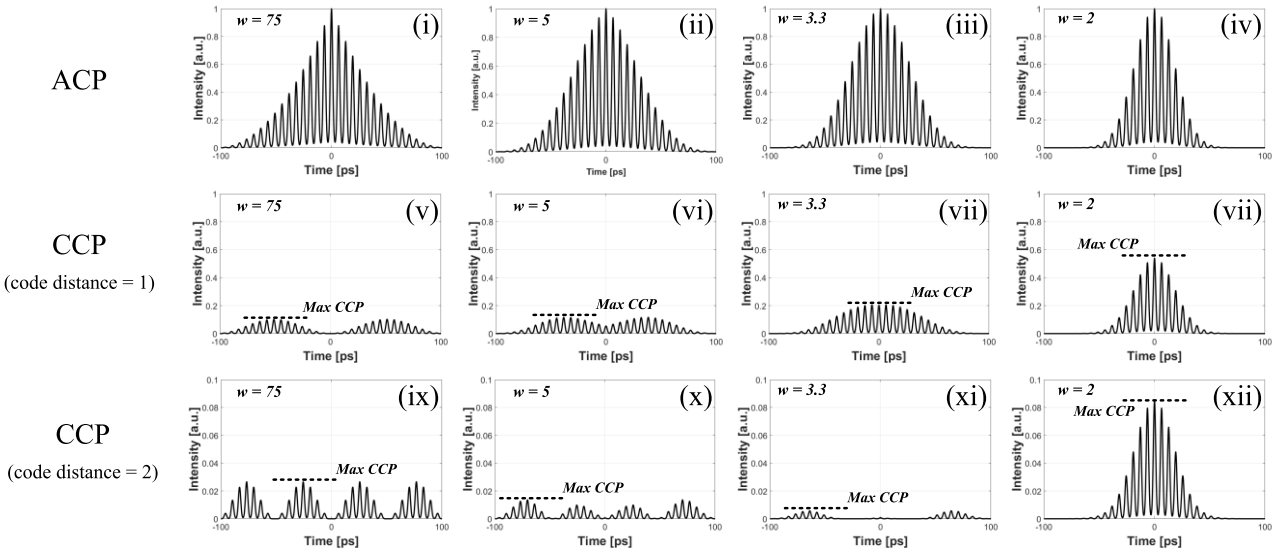

FIGURE 2. Normalized ACP and CCP signals with different Gaussian RMS width.

Throughout this paper, the SBR is set to 0.8 in order to avoid the interference between the correctly decoded adjacent signals.

Since the single ultra-short pulse has been processed by the encoder, the output signal of the AS-OCDM encoder is the series of N short optical pulses. The amplitude and the phase pattern of each chip is governed by,

$$E_{code-c}(t) = \sum_{k=0}^{N-1} \sqrt{g(k+1)} \times \exp\left[-j\frac{2\pi k}{N}(c-1)\right] \times \exp\left[-\frac{(t-k\,(T_{bit}\cdot SBR/N))^2}{2T_0^2}\right]. \quad (4)$$

At the decoding process, the correlation between the encoded signal $E_{code-c}(t)$ and the impulse response $h_{code-c}(t)$ of the decoder result a decoded signal. The correctly and the incorrectly decoded signals become the auto-correlation peak signal (ACP) and the cross-correlation peak signal (CCP), respectively [17]. We evaluate the normalized ACP and CCP waveforms from a 16-chip en/decoder of the conventional OCDM and the AS-OCDM with different shaping profiles, obtained from the computational software as shown in Fig. 2. We can see in inset (i) that the ACP of the unshaped OCDM looks like a triangle-shape, while the ACPs in insets (ii)-(iv) of the AS-OCDM form Gaussian shapes, which are the outcomes from shaping profile in (1). The CCP waveform is depended on the code distance between the code of the decoder and the target code. For example, when the target code is code #3 and the code of the decoder is code #4, the code distance is equivalent to 1. The waveforms of the CCPs with code distance = 1 are shown in insets (v)-(viii). Moreover, for the case of the code distance = 2, the CCP waveforms are shown in insets (ix)-(xii). By shaping the OCDM waveforms, in insets (v)-(viii), the shapes of the CCP signal transform two big lobes into single lobe with bell-shape as we reduce the width of the shaping profile. Moreover, the maximum amplitudes of the CCPs increase, in comparison with their ACP, they are all larger than the unshaped OCDM. On the other hand, for the case of the code distance is 2, the CCP waveform transforms 4 equally small lobes into 2 small side-lobes with a very small center lobe, when we reduced the width to 3.3, as shown in inset (xi). The maximum amplitude of the CCP is also reduced. Nevertheless, in a case when we continue reducing the width, the CCP finally becomes a single-lobe with bell-shape, and the maximum CCP increases, as shown in inset (xii). Since most of the conventional OCDM systems use the multi-level phase-shifted code employing unshaped encoded signal, we show that the system performance can be improved by shaping the amplitude of the OCDM signal.

III. AMPLITUDE-SHAPING OCDM CODE DETECTION PERFORMANCE

In this section, we show the code detection performance of both the conventional OCDM and the AS-OCDM. The first parameter is the auto-correlation intensity peak to the maximum cross-correlation ratio (P/C). The second one is the power contrast ratio (PCR) [25], [26], and the last one is the total power contrast ratio considering all subscribers using non-adjacent codes, respectively. For the case of using the 16-chip en/decoder, the parameters a and b in (1) are set to be 1, and 8.5, respectively.

A. AUTO-CORRELATION INTENSITY PEAK TO THE MAXIMUM CROSS-CORRELATION RATIO

The P/C ratio is defined as the different level between the maximum peak of the ACP and the maximum peak of the

CCP. We calculate the P/C ratio from,

$$P/C = \frac{ACP^2}{CCP^2}. \tag{5}$$

We investigate the P/C ratio as a function of the width of the shaping profile from 0 to 100. The P/C ratios are illustrated in Fig. 3. The black solid line shows the P/C ratio for the case of using adjacent codes (distance between code is 1). We found that the P/C ratio increases with w, then it converges to 9.89 dB since w is larger than 20. We also found that the amplitudes of all 16 chips of the normalized encoded signal are converged to 1 as well. Therefore, we can assume the AS-OCDM with the width larger than 20 as the conventional OCDM system. For the case of the code distance is 2, shown in black dotted-line, The P/C ratio increases to the maximum at 23.69 dB with $w = 3$. After this point, the P/C ratio decreases and converges to 15.74 dB as w increases. Similarly, the P/C ratio of the code-distance $= 3$ reaches the maximum of 36.21 dB at $w = 2.5$. Then the P/C ratio decreases as a function of w, and finally converged to 18.98 dB, respectively.

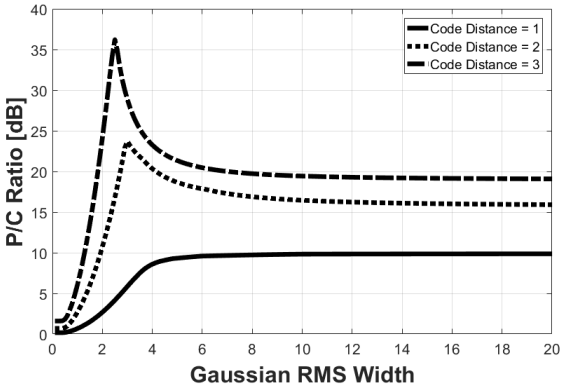

FIGURE 3. P/C ratio as a function of Gaussian RMS width.

B. POWER CONTRAST RATIO

The power contrast ratio (PCR) is defined as the ratio between the average power of the ACP waveform and the average power of the CCP waveform. We calculate the PCR from,

$$PCR_j = 10\log\left(\frac{P_{ccp-j}}{P_{acp}}\right), \tag{6}$$

where j is the code number of the interfered subscribers ($j \neq c$). The average power of P_{acp}, and P_{ccp-j} can be calculated by using (3) in [25].

We show the relation between the PCR as a function of w in Fig. 4, for the case of the code distances are 1-4. The large negative value of the PCR represents the great code-detection capabilities between en/decoders. We can see that, by using the AS method to reduce the width of the shaping profile, the PCR for the case of code distance $= 1$ is worse than the conventional system. On the other hand, the avoidance of using the adjacent code, the PCR is improved and the optimal

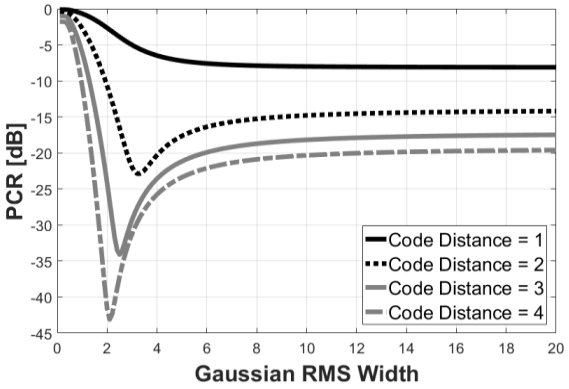

FIGURE 4. PCR as a function of Gaussian RMS width.

points are 3.3, 2.5, and 2.1 with PCR $= -22.88$, -34.10, and -43.11 dB, for the case of code distances are 2-4, respectively.

C. TOTAL POWER CONTRAST RATIO

In the multi-subscriber OCDM signal transmission, all signals from the subscribers are multiplexed together. Since the PCR of the adjacent code is poor (approximately -7 dB for 16-chip en/decoder), the serious PBN and MAI cause severe waveform fluctuation at the receiver. We usually avoid using the adjacent codes. Therefore, for the case of using the 16-chip en/decoder, 8 codes are normally multiplexed simultaneously with the odd code-set (#1, #3, . . ., #15) or the even code-set (#2, #4, . . ., #16). The total PCR is the ratio between the sum of all P_{ccp-j} and P_{acp}, as shown by,

$$PCR_{total} = \frac{\sum_{i=1}^{m} P_{ccp-i,j}}{P_{acp}}. \tag{7}$$

The index i is the number of the interfered subscriber using code #j in the code set, and m is the total number of interfered subscribers. We investigate the PCR_{total} as a function of w with total 8 subscribers employing the odd code set. The numerical result is shown in Fig. 5. It is shown that the optimal point of w is equals to 3.3 with PCR_{total} of -18.25 dB.

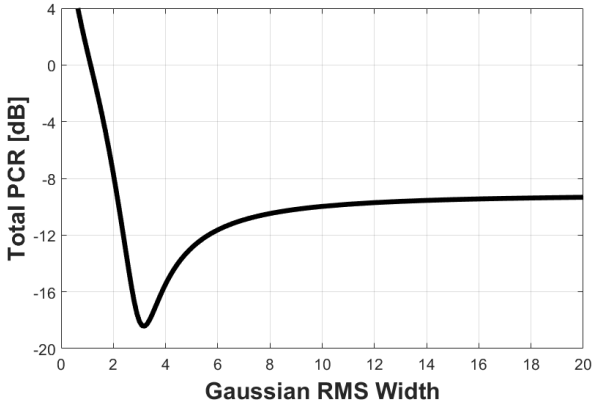

FIGURE 5. Relation between total PCR and Gaussian RMS width.

This figure also shows that, by using the AS-OCDM, can improve the PCR_{total}, in comparison to the conventional OCDM in which its PCR_{total} is approximately converged to −9.13 dB.

IV. SYSTEM PERFORMANCE

To evaluate the system performance, the conventional and the AS-OCDM system with 16-chip en/decoder at a data rate of 10 Gbps is theoretically calculated by using the computational software. Total 8 OCDM subscribers are multiplexed together using the odd code set. The system architecture is shown in Fig. 6, without considering the dispersion effect.

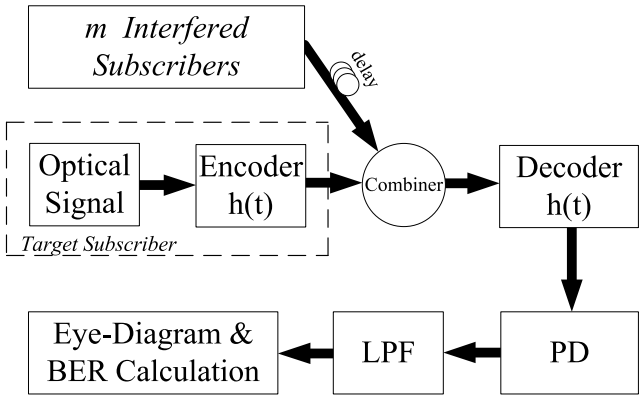

FIGURE 6. System block diagram for the system performance analysis.

The simple architecture of the optical en/decoder is shown in Fig. 7. For simplification, we illustrate the figure for the case of 8-chip en/decoder based on the planar lightwave circuit (PLC) device obtained from [29, Fig. 1]. The short optical pulse is equally split into 8 branches. In each branch of the en/decoder, there is a variable optical attenuator (VOA), a phase shifter, and a delay. The pulse with a specific amplitude, a phase, and a delay governed by (4), will be combined by a combiner. It should be noted that, for the conventional OCDM, we do not apply the VOA so that we obtain the encoded signal with the same amplitudes. On the other hand, a specific value of the VOA should be added to each branch for the shaping purpose. As a result, the shaped encoded signal with the desired shaping-profile can be achieved.

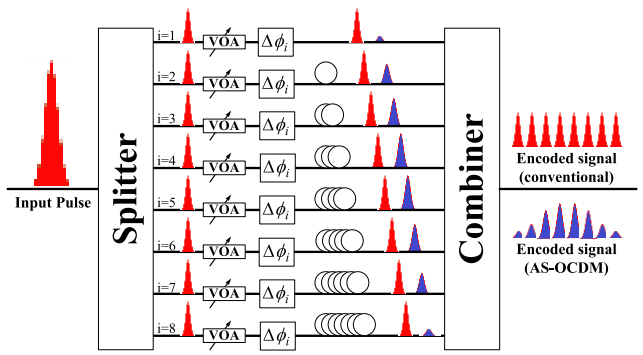

FIGURE 7. Optical en/decoder architecture of the conventional and the AS-OCDM.

After the decoding process, the detected signal $E_{PIN}(t)$ at the PIN photodetector (PD) is the mixture of the optical field from the desired ACP and the total number of m interfered CCP signals can be expressed as,

$$E_{PIN}(t) = E_{acp}(t) + \sum_{i=1}^{m} E_{ccp-i}(t). \tag{8}$$

By the square-law detection, the decision signal Z from the period T after being detected by PIN is,

$$\begin{aligned} Z = R \cdot \int_0^T E_{acp}(t) \cdot E^*_{acp}(t)dt + R \cdot \sum_{i=1}^{m} \int_0^T E_{ccp-i}(t) \\ \cdot E^*_{ccp-i}(t)dt + 2R \cdot \sum_{i=1}^{m} \int_0^T E_{acp}(t) \cdot E^*_{ccp-i}(t)dt + 2R \\ \cdot \sum_{j=i+1}^{m} \sum_{i=1}^{m-1} \int_0^T E_{ccp-i}(t) \cdot E^*_{ccp-j}(t)dt + \int_0^T n_0(t)dt. \end{aligned} \tag{9}$$

The factor R is the responsivity of PIN photodetector. The first term in (9) is the desired ACP. The second term is the MAI noise. The third term is the PBN. The fourth term is the secondary beat noise (SBN), and the last term refers to the Gaussian random noise at receiver with variance σ^2_{rx}, which is resulted from to the thermal noise, the shot noise and the dark current noise, respectively. The variance of the thermal noise, the shot noise, and the dark current noise, can be calculated from [25],

$$\sigma^2_{th} = \frac{4k_B BT}{R_L}, \tag{10}$$

$$\sigma^2_{sh} = 2qBRP_{acp}\,(1 + PCR_{total}), \tag{11}$$

$$\sigma^2_{d} = 2qBI_d, \tag{12}$$

where k_B is the Boltzmann's constant, B is the bandwidth of receiver, T is the temperature, R_L is the load resistance, q is the electron charge, and I_d is the dark current, respectively.

We assume the calculation under the worst-case scenario, when the highest peak of each CCP is aligned at the center of the ACP by adjusting an appropriate delayed time to each subscriber. As a result, the waveform fluctuation of the desired signal at the receiver can be obtained from the largest value of the PBN. The variance of the PBN, considering the random bit phase between the ACP and the CCP shown in (13) refers to [29],

$$\sigma^2_{PBN} = \frac{R^2}{T} \sum_{i=1}^{m} \int_0^{2\pi} \int_0^{T_{bit}} \left(E^2_{acp}(t) \cdot E^2_{ccp-i}(t) \cdot \cos^2\theta_i \right) \times dtd\theta_i. \tag{13}$$

The total noise variances for the bit "0", and "1" are,

$$\sigma^2_0 = \sigma^2_{MAI} + \sigma^2_{SBN} + \sigma^2_{Rx}, \tag{14}$$

$$\sigma^2_1 = \sigma^2_{MAI} + \sigma^2_{SBN} + \sigma^2_{PBN} + \sigma^2_{Rx}. \tag{15}$$

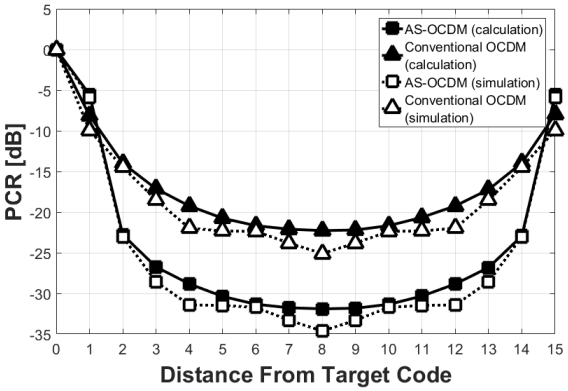

FIGURE 8. PCR of the conventional and the AS-OCDM system.

Finally, we investigate the system performance by using the classical BER calculation. The BER of the OCDM system, stated in [25], is expressed as

$$BER = \frac{1}{4}\left(erfc\left[\frac{RP_{acp}\,(1 + PCR_{total} - I_D)}{\sqrt{2}\sigma_1}\right] + erfc\left[\frac{RP_{acp}\,(I_D - PCR_{total})}{\sqrt{2}\sigma_0}\right]\right). \quad (16)$$

The threshold decision level I_D is optimized by,

$$I_D = \frac{(\sigma_0 \cdot (1 + PCR_{total})) + (\sigma_1 \cdot PCR_{total})}{\sigma_0 + \sigma_1}. \quad (17)$$

We perform the calculation with all parameters declared in Table 1. Since the optimum w that can achieve the lowest PCR_{total} is equal to 3.3. We use this value for the AS-OCDM to evaluate the system performance. For the case of conventional OCDM, w is set as 75, respectively. As a result, the calculated PCR is shown in Fig. 8. We can see that, with code distance = 1, the PCR of the AS-OCDM (−5.56 dB) is worse than the conventional system (−8.14 dB). However, in the case that the code distance is greater than 1, the AS-OCDM with the optimum value of w can improve the PCR.

TABLE 1. Parameters used in the calculation and simulation.

Parameter	Value
Total simulated bits	1024 Bits
Samples per bit	2048 Samples
System data rate	10 Gbps
w	3.3 (AS-OCDM) 75 (conventional)
T_{bit}	100 ps
Optical pulse width	2 ps
Pulse repetition rate	10 GHz
Optical modulator	Intensity modulator
Extinction ratio	20 dB
N	16
t_{chip}	5 ps
R	0.85 A/W
k_B	1.38×10^{-23} J/K
B	7.5 GHz
T	300 K
R_L	50 Ohms
q	1.6×10^{-19} C
I_d	10 nA

The numerical BER, calculated from (16), as a function of received optical power (ROP) is illustrated in Fig. 9. It should be noted that the BER can be considered as the error-free transmission in a case that the BER is lower than the FEC limit at BER = 10^{-3}. The conventional system, for the case of 8 subscribers, the BER has an error floor around 10^{-4}. The maximum ROP and the power penalty compared with the 1-subscriber case, at the FEC limit, are −20.53 dBm, and 4.66 dB, respectively. The inset (i) in Fig. 9(a) shows the eye-diagram at the FEC limit. The waveform fluctuation is severe since the interference in this case is mainly caused by the PBN and MAI. On the contrary, with the help of the AS technique,

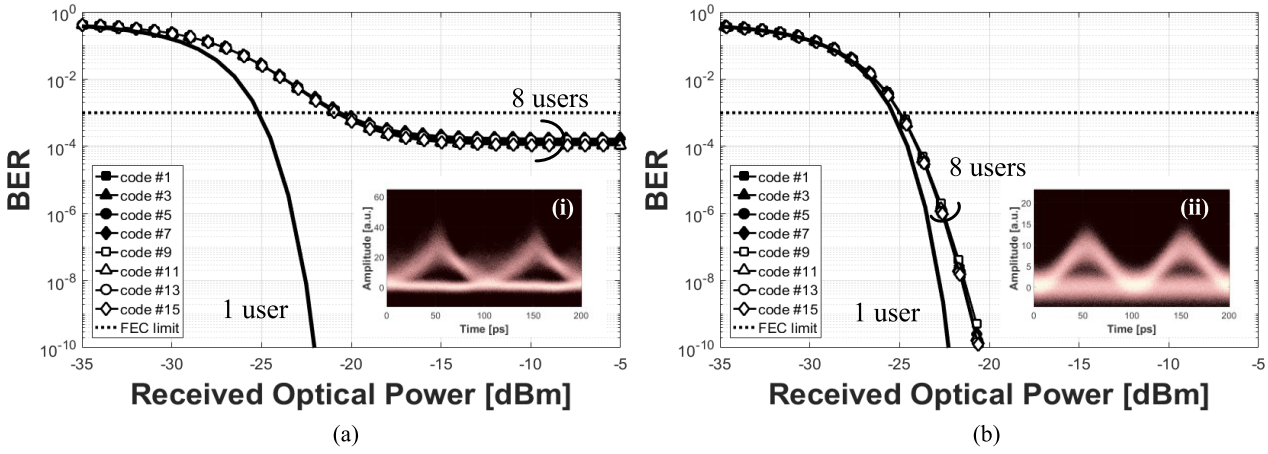

FIGURE 9. Numerical BER of 1 and 8-subscribers case, (a) Conventional-OCDM, and (b) AS-OCDM.

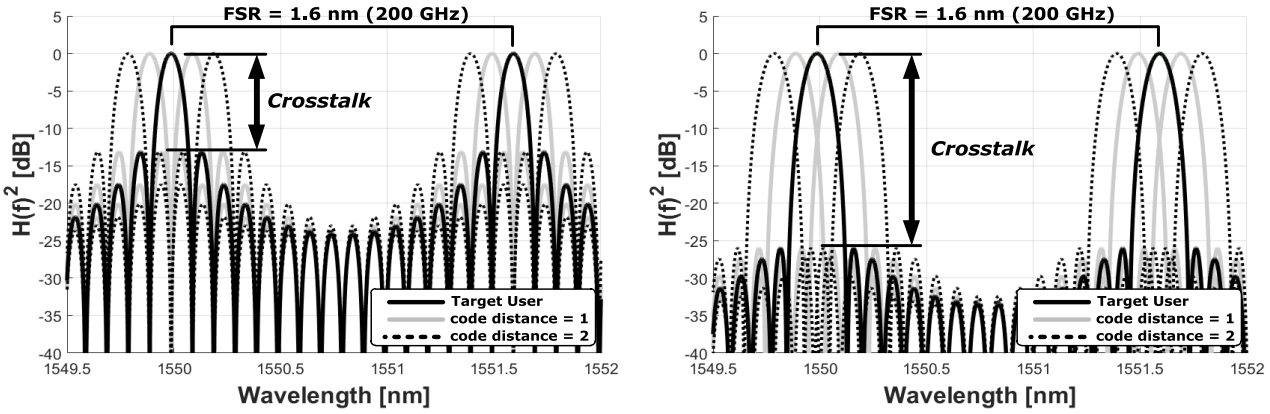

FIGURE 10. Calculated spectra of the optical code, (a) Conventional-OCDM, and (b) AS-OCDM.

the maximum ROP for 8-subscribers case, at the FEC limit, is improved to −24.95 dBm and the power penalty is 0.45 dB as shown in Fig. 9(b). All BERs have the error-floor lower than 10^{-12}. The eye-diagram shown in inset (ii) illustrates a lower fluctuation in comparison to inset (i) because the reduction of the CCP, by employing AS-OCDM, can reduce the PBN and MAI, respectively.

The calculated spectra are shown in Fig. 10. By using AS-OCDM, the spectral components of the interfered subscribers using the code distance = 2 (black-dotted line) inside the bandwidth of the target code are reduced. As a result, we can mitigate the crosstalk from the PBN and the MAI. However, the AS-OCDM cannot suppress the spectral components of the interfered subscribers using code distance = 1 (the grey solid line).

V. SIMULATION RESULTS

We verify the numerical results in section IV with the computer simulation by using Optisystem. The system block diagram is the same as Fig. 6. The optical transmitter transmits 2-ps optical pulses whose center wavelength is 1550 nm, at a repetition rate of 10 GHz. These optical pulses are modulated with the pseudo-random bit sequence (PRBS) 2^{10}-1 bits by using the intensity modulator with the extinction ratio of 20 dB to obtain the OOK data format. All optical signal processing is performed by a programmable 16-chip multi-level phase-shifted keying en/decoder. The simple block diagram of the en/decoder is shown in Fig. 7. For the case of the AS-OCDM, the VOA is inserted to each branch of the en/decoder in order to shape the amplitude of the optical signal to the desired level. For the case of $w = 3.3$, the attenuations for branch #1-#8 are 11.17, 8.37, 5.98, 3.99, 2.39, 1.19, 0.39, and 0 dB, respectively. For branch #9-#16, the attenuations are added in the reverse order to obtain the symmetrical shaping signal. On the other hand, it is not necessary to apply the VOA at the en/decoder in the conventional system. All 8 encoded signals employing the odd code-set are combined by an optical power combiner. Additional optical delays are added to obtain the worst case scenario which the highest peak of each CCP is aligned at the center of the ACP. At the receiver side, the optical signals are decoded individually and are converted to the electrical signals with the photodetectors. Then, the signals are filtered by a low-pass filter. All parameters used in the simulation are stated in Table 1. Finally, the BER of the received signals are measured by using the eye-diagram analyzer.

We measure the PCR by measuring the optical power of the decoded signals in front of the PD, in the Optisystem software. The results are fitted with the numerical calculation results in section IV as shown in Fig. 8. The PCRs of the conventional OCDM are −9.95, and −14.47 dB for the case of the code distances are 1, and 2, respectively. The PCR of the AS-OCDM with the adjacent code is −5.88 dB, higher than the conventional OCDM. Nevertheless, for the case of code distance = 2, the PCR is −23.04 dB which is better than the conventional OCDM.

The BER as a function of the ROP obtained from the simulation is shown in Fig. 11. In Fig. 11(a), the BER of the 1 and 8-subscribers can achieve the FEC limit with the maximum ROP of −21.89, and −20.39 dBm, respectively. The power penalty caused by PBN and MAI is 1.5 dB. The eye-diagram of the signal at the FEC limit is shown in inset (i). For AS-OCDM, the BER is shown in Fig. 11(b). The maximum ROP at the FEC limit is −22.62 dBm for the case of 1 subscriber. It is better than the conventional OCDM by 0.73 dB because the ACP of the AS-OCDM can achieve the same peak amplitude as the conventional OCDM with lower average power. In the 8-subscribers case, the maximum ROP at the FEC limit is −22.05 dBm, and the eye-diagram is shown in inset (ii), respectively. The power penalty in comparison with the 1-subscriber case is 0.57 dB. The AS-OCDM with the optimal shaping profile can enhance the code detection performance, and the maximum ROP at the FEC limit, so that the effect of the PBN and MAI is negligible. The simulation

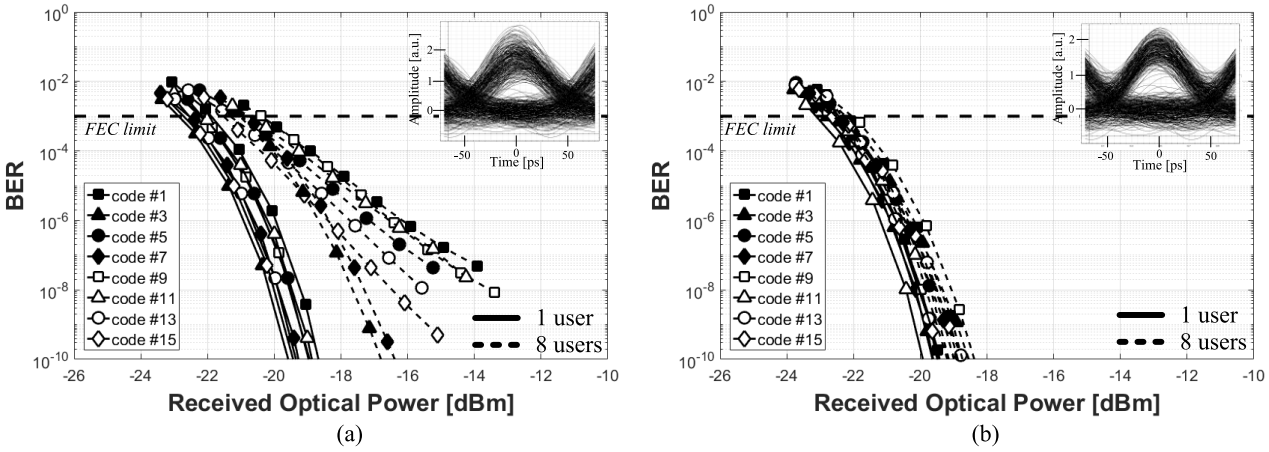

FIGURE 11. BER from the simulation, (a) Conventional-OCDM, and (b) AS-OCDM.

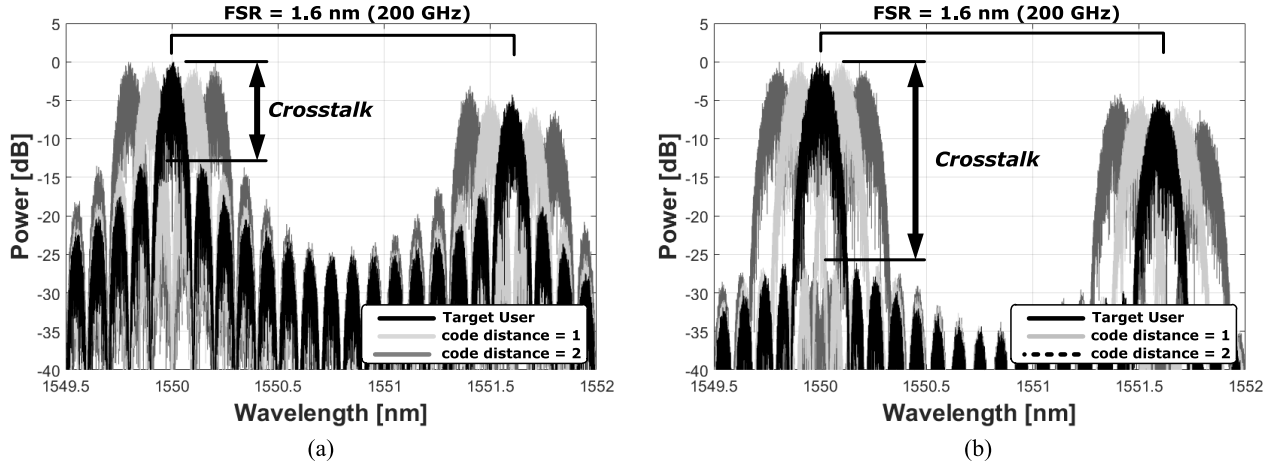

FIGURE 12. Simulated optical spectra of the correctly decoded signal, (a) Conventional-OCDM, and (b) AS-OCDM.

results also confirm the numerical result that it is possible to reduce the PBN and the MAI by shaping the en/decoded signals. The simulated spectra of the correctly decoded signal are shown in Fig. 12. Furthermore, these simulated spectra strengthen our numerical spectra shown in Fig. 10 that we can reduce the crosstalk by using the AS-OCDM technique.

VI. CONCLUSION

This paper has proposed the AS technique for a 10-Gbps coherent time-spreading OCDM system based OOK data format with 16-multi level phase-shifted en/decoder. The impulse response of the en/decoder was modified in order to return the en/decoded signal with the desired amplitudes which were governed by the Gaussian shaping profile. With this technique, the code detection performance, the P/C ratio, the PCR, and the total PCR were improved. As a result, the signal distortion mainly caused by the PBN and the MAI was negligible. The numerical results showed that the proposed AS-OCDM with the optimal shaping profile could improve the BER for the case of 8-subscribers. The maximum ROP at the FEC limit, without considering the effect of chromatic dispersion, was improved by 4.21 dB in comparison with the conventional system. We also confirmed the numerical results by a computer simulation. The block diagram of the AS-OCDM en/decoder was shown with the simple architecture of the PLC. The PCR, the BER, and the maximum ROP at the FEC limit of 8-subscribers case were improved and in a good agreement with the numerical results. From our results, we believe that our pilot work can be a guideline for further researches, as well as the implementation on the AS-OCDM en/decoders.

ACKNOWLEDGMENT

The authors would like to thank all of the anonymous reviewers for their careful reading, valuable comments, and suggestions.

REFERENCES

[1] G. Finnie. (Jan. 2005). *FTTH in Europe: Forecast & Prognosis 2006-2011*. [Online]. Available: http://www.ftthcouncil.eu/documents/Reports/Market_Forecast_January_2005.pdf

[2] K. Kitayama *et al.*, "Photonic network vision 2020—Toward smart photonic cloud," *J. Lightw. Technol.*, vol. 32, no. 16, pp. 2760–2770, Aug. 15, 2014.
[3] T. Asai, "5G radio access network and its requirements on mobile optical network," in *Proc. Int. Conf. Opt. Netw. Design Modeling*, Pisa, Italy, May 2015, pp. 7–11.
[4] *Cisco Visual Networking Index: Global Mobile Data Traffic Forecast Update, 2016–2021 White Paper*, document C11-481360-01, Cisco Systems, San Jose, CA, USA, 2014, pp. 1–17.
[5] E. Wong, "Next-generation broadband access networks and technologies," *J. Lightw. Technol.*, vol. 30, no. 4, pp. 597–608, Feb. 15, 2012.
[6] J. Kani, J. Terada, K.-I. Suzuki, and A. Otaka, "Solutions for future mobile fronthaul and access-network convergence," *J. Lightw. Technol.*, vol. 35, no. 3, pp. 527–534, Feb. 1, 2017.
[7] J. Terada, T. Shimada, T. Shimizu, and A. Otaka, "Optical network technologies for wireless communication network," in *Proc. Eur. Conf. Opt. Commun. (ECOC)*, Dusseldorf, Germany, Sep. 2016, pp. 1–3, Paper Tu.1.F.2.
[8] N. Suzuki, H. Miura, K. Matsuda, R. Matsumoto, and K. Motoshima, "100G to 1T based coherent PON technology," in *Proc. Eur. Conf. Opt. Commun. (ECOC)*, Gothenburg, Sweden, Sep. 2017, pp. 1–3, Paper Th.1.B.1.
[9] Y. Luo *et al.*, "Time- and wavelength-division multiplexed passive optical network (TWDM-PON) for next-generation PON stage 2 (NG-PON2)," *J. Lightw. Technol.*, vol. 31, no. 4, pp. 587–593, Feb. 15, 2013.
[10] D. Nesset, "NG-PON2 technology and standards," *J. Lightw. Technol.*, vol. 33, no. 5, pp. 1136–1143, Mar. 2015.
[11] (2017). *IEEE P802.3ca Task Force*. [Online]. Available: http://www.ieee802.org/3/ca
[12] C. Knittle, "IEEE 100 Gb/s EPON," in *Proc. Opt. Fiber Commun. Conf. Exhib.*, Anaheim, CA, USA, Mar. 2016, pp. 1–3, Paper Th1I.6.
[13] R. Matsumoto *et al.*, "40G-OCDMA-PON system with an asymmetric structure using a single multi-port and sampled SSFBG encoder/decoders," *J. Lightw. Technol.*, vol. 32, no. 6, pp. 1132–1143, Mar. 15, 2014.
[14] P. R. Prucnal, *Optical Code Division Multiple Access*, 1st ed. Boca Raton, FL, USA: CRC Press, 2005.
[15] K. Kitayama, X. Wang, and N. Wada, "OCDMA over WDM PON-solution path to gigabit-symmetric FTTH," *J. Lightw. Technol.*, vol. 24, no. 4, pp. 1654–1662, Apr. 2006.
[16] S. Mhatli, H. Mrabet, E. Giacoumidis, and I. Dayoub, "Performance evaluation of an IMDD optical OFDM-CDMA system," *Appl. Opt.*, vol. 57, no. 7, pp. 1569–1574, Mar. 2018.
[17] G. Cincotti, N. Wada, and K. Kitayama, "Characterization of a full encoder/decoder in the AWG configuration for code-based photonic routers-part I: Modeling and design," *J. Lightw. Technol.*, vol. 24, no. 1, pp. 103–112, Jan. 2006.
[18] N. Kataoka *et al.*, "Field Trial of Duplex, 10 Gbps×8-user DPSK-OCDMA system using a single 16×16 multi-port encoder/decoder and 16-level phase-shifted SSFBG encoder/decoders," *J. Lightw. Technol.*, vol. 27, no. 3, pp. 299–305, Feb. 1, 2009.
[19] X. Wang, N. Wada, T. Miyazaki, G. Cincotti, and K. Kitayama, "Field trial of 3-WDM×10-OCDMA×10.71-Gb/s asynchronous WDM/DPSK-OCDMA using hybrid E/D without FEC and optical thresholding," *J. Lightw. Technol.*, vol. 25, no. 1, pp. 207–215, Jan. 2007.
[20] T. Kodama *et al.*, "Scaling the system capacity and reach of a 10G-TDM-OCDM-PON system without an en/decoder at an ONU," *IEEE/OSA J. Opt. Commun. Netw.*, vol. 5, no. 2, pp. 134–143, Feb. 2013.
[21] N. Kataoka, G. Cincotti, N. Wada, and K. Kitayama, "2.56 Tbps (40-Gbps×8-wavelength×4-OC×2-POL) asynchronous WDM-OCDMA PON using a multi-port encoder/decoder," in *Proc. 37th Eur. Conf. Exhib. Opt. Commun.*, Sep. 2011, pp. 1–3, Paper Th.13.B.6.
[22] X. Wang and K. Kitayama, "Analysis of beat noise in coherent and incoherent time-spreading OCDMA," *J. Lightw. Technol.*, vol. 22, no. 10, pp. 2226–2235, Oct. 2004.
[23] W. Amaya, D. Pastor, and J. Capmany, "Modeling of a time-spreading OCDMA system including nonperfect time gating, optical thresholding, and fully asynchronous signal/interference overlapping," *J. Lightw. Technol.*, vol. 26, no. 7, pp. 768–776, Apr. 1, 2008.
[24] R. Matsumoto *et al.*, "Apodized SSFBG encoder/decoder for 40G-OCDMA-PON system," in *Proc. 8th OptoElectron. Commun. Conf.*, Kyoto, Japan, Jun./Jul. 2013, pp. 1–2, Paper PDP MP1-6.
[25] T. Kodama, N. Wada, G. Cincotti, and K.-I. Kitayama, "Asynchronous OCDM-based 10 G-PON using cascaded multiport E/Ds to suppress MAI noise," *J. Lightw. Technol.*, vol. 31, no. 20, pp. 3258–3266, Oct. 15, 2013.
[26] T. Kodama, N. Wada, G. Cincotti, X. Wang, and K.-I. Kitayama, "Noise suppression using optimum filtering of OCs generated by a multi-port encoder/decoder," *Opt. Express*, vol. 20, no. 9, pp. 10320–10329, Apr. 2012.
[27] M. Mackenzie and K. Tieu, "Gaussian filters and filter synthesis using a Hermite/Laguerre neural network," *IEEE Trans. Neural Netw.*, vol. 15, no. 1, pp. 206–214, Jan. 2004.
[28] A. M. Kusters, M. Glade, and K. Heime, "Carrier lifetime measurement in semiconductor lasers using injection current pulses of Gaussian shape," *IEEE J. Quantum Electron.*, vol. 28, no. 12, pp. 2669–2673, Dec. 1992.
[29] G. Manzacca, A. M. Vegni, X. Wang, N. Wada, G. Cincotti, and K. I. Kitayama, "Performance analysis of a multiport encoder/decoder in OCDMA scenario," *IEEE J. Sel. Topics Quantum Electron.*, vol. 13, no. 5, pp. 1415–1421, Sep. 2007.

RACHATA MANEEKUT received the B.E. and M.E. degrees from Chulalongkorn University, Thailand, in 2007 and 2010, respectively, where he is currently pursuing the Ph.D. degree in microwave and lightwave communications strategic research area with the Department of Electrical Engineering, Faculty of Engineering. In 2017, he joined the Internship Program at the Photonic Transport Network Laboratory, KDDI Research, Japan. His research interests include the advance modulation scheme over passive optical network, optical signal processing, and the next-generation optical elastic network technology. In 2015, he received the short-term research fellowship from the National Institute of Information and Communications Technology, Japan.

PASU KAEWPLUNG was born in Bangkok, Thailand, in 1971. He received the B.S. and M.S. degrees in electrical engineering from Yokohama National University, Yokohama, Japan, in 1996 and 1998, respectively, and the Ph.D. degree in electrical engineering from Chulalongkorn University in 2003. From 1998 to 2000, he conducted research at the Research Center for Advanced Science and Technology, The University of Tokyo, Japan. He is currently an Assistant Professor in the microwave and lightwave communications strategic research area with the Department of Electrical Engineering, Faculty of Engineering, Chulalongkorn University. His research activities have been devoted to optical access technology, optical fiber transmission systems, dispersion management, and the applications of nonlinear optical effects.